

# Flow patterns in the sedimentation of an elliptical particle

ZHENHUA XIA<sup>1,2</sup>, KEVIN W. CONNINGTON<sup>2</sup>,  
SAIKIRAN RAPAKA<sup>2</sup>, PENGTAO YUE<sup>3</sup>, JAMES J. FENG<sup>3</sup>  
AND SHIYI CHEN<sup>1,2†</sup>

<sup>1</sup>State Key Laboratory for Turbulence & Complex Systems, CAPT and CCST, College of Engineering,  
Peking University, Beijing, China

<sup>2</sup>Department of Mechanical Engineering, The Johns Hopkins University, Baltimore, MD 21218, USA

<sup>3</sup>Department of Chemical and Biological Engineering and Department of Mathematics,  
University of British Columbia, Vancouver, BC Canada V6T 1Z3

(Received 10 June 2008 and in revised form 5 December 2008)

We study the dynamics of a single two-dimensional elliptical particle sedimenting in a Newtonian fluid using numerical simulations. The main emphasis in this work is to study the effect of boundaries on the flow patterns observed during sedimentation. The simulations were performed using a multi-block lattice Boltzmann method as well as a finite-element technique and the results are shown to be consistent. We have conducted a detailed study on the effects of density ratio, aspect ratio and the channel blockage ratio on the flow patterns during sedimentation. As the channel blockage ratio is varied, our results show that there are five distinct modes of sedimentation: oscillating, tumbling along the wall, vertical sedimentation, horizontal sedimentation and an inclined mode where the particle sediments with a non-trivial orientation to the vertical. The inclined mode is shown to form a smooth bridge between the vertical and horizontal modes of sedimentation. For narrow channels, the mode of sedimentation is found to be sensitively dependent on the initial orientation of the particle. We present a phase diagram showing the transitions between the various modes of sedimentation with changing blockage ratio of the channel.

---

## 1. Introduction

There are many naturally occurring situations and industrial applications that involve the transport of inertial sized solid particles in a viscous fluid. Blood flow, slurries and colloids are some of the cases where neither the carrier fluid nor the suspended solid particle inertia can be neglected. In these situations, the Reynolds number is moderate, and the behaviour of the solid and fluid are coupled, and one must explicitly account for their mutual interaction when performing a computational simulation.

Several authors (see Brady & Bossis 1985; Sugihara-Seki 1993) have employed quasi-steady methods, ignoring transient effects of particle and fluid inertia, for simulating moving particles in creeping flows. Feng & Joseph (1995) demonstrated that even in low-Reynolds-number flows, there may be situations where inclusion of the transient terms alters the nature of the motion. They concluded that factors such

† Email address for correspondence: saikiran@jhu.edu, syc@jhu.edu

as ‘the unsteadiness of the quasi-steady Stokes motion, the nature of periodicity in the basic solution and wall effects’ present situations where disregarding the transient terms leads to a qualitatively erroneous prediction of the flow character for quasi-steady methods. Feng pointed out that ‘walls tend to enhance the unsteady inertial effects and make quasi-steady solutions unstable to temporal disturbances imposed by the transient terms’. For simulations where wall effects dictate the complexion of the flow, it is compulsory to employ methods that account for transient terms, even for small-Reynolds-number flows, and to question the precarious integrity of results computed without those terms.

Several authors (see Hu, Joseph & Crochet 1992; Feng, Hu & Joseph 1994*a, b*; Huang, Feng & Joseph 1994; Hu 1995, 1996; Huang, Hu & Joseph 1998) studied solid–fluid suspensions with inertia using the finite-element method. While their technique captures the coupled interaction between the solid and the fluid phases, it can become computationally expensive. The translation and rotation of the solid particle involves regeneration of the mesh and projection of the fluid variables from the old to new mesh whenever the grid becomes too distorted. Physalis (Prosperetti & Oguz 2001) is another method that is capable of handling these types of simulations, though the analytical solution required near the particle surface restricts its use to particles of simple shape – essentially circular particles. Uhlmann (2005) has extended the immersed boundary method (Lai & Peskin 2000; Mittal & Iaccarino 2005) to simulate flows with rigid particles. As an auspicious alternative, the lattice Boltzmann method (LBM) (Frisch *et al.* 1987; Chen & Doolen 1998) became a popular tool for simulating solid particle suspensions (Ladd 1994*a, b*; Aidun & Lu 1995; Aidun, Lu & Ding 1998; Qi 1999; Ladd & Verberg 2001; Feng & Michaelides 2004). In the LBM, the solid particles are mapped onto the fluid domain, defined on a stationary Cartesian grid. The discrete Boltzmann equation is solved in the fluid domain, where the Navier–Stokes equations are recovered through a multi-scaling expansion procedure. (Ladd 1994*a, b*) was the first to use the LBM to simulate solid particle suspensions, as he enhanced the standard bounce-back method to account for moving boundaries. The force and torque are calculated on the surface of the particle, whose position and velocity is updated according to Newtonian dynamics. There is no need to re-mesh the stationary grid as the particles move, economizing the computational cost of the simulation.

In this paper, we shall use the LBM to discuss some previously undisclosed features of two-dimensional elliptical particle sedimentation in a narrow channel. Though there have been many erudite studies of elliptical and ellipsoidal particle behaviour in Couette and Poiseuille flows (see Feng *et al.* 1994*b*; Feng, Huang & Joseph 1995; Ding & Aidun 2000; Qi *et al.* 2002), this discourse will focus on two-dimensional sedimentation. An ostensibly innocent problem, elliptical particle sedimentation is teeming with latent physical phenomena.

Feng *et al.* (1994*a*) demonstrated that an ellipse which settles between parallel walls will translate to the centre of the channel due to wall effects and orient itself so that its major axis is orthogonal to the direction of gravity for any initial configuration. They grouped the behaviour of the ellipse into four different regimes based on increasing Reynolds number: (a) approach to stable configuration which does not overshoot; (b) overshoot in both lateral and angular coordinates with eventual steady state at stable configuration; (c) periodic oscillation about stable configuration due to periodic swing of attached eddies prior to vortex shedding; (d) enhanced oscillation about stable configuration due to vortex shedding. These regimes were described for Reynolds numbers up to 345. Adjusting the blockage ratio altered the Reynolds

number intervals these regimes occurred in. Increasing the Reynolds number further led to a chaotic tumbling motion. One interesting disparity between a circular and an elliptical particle at a Reynolds number high enough is that the circular particle will establish its lateral equilibrium position off centre, stabilized by a unidirectional rotation. A stabilizing pressure couple does not allow the ellipse to achieve this rotation, thus resigning the particle to oscillation about the centre.

Huang *et al.* (1994) analysed the turning couples on an ellipse in the regime where there is oscillation due to vortex shedding. They calculated the distributions of pressure and shear stress on the surface of the particle and separated the total torque into their respective contributions. They concluded that high pressure at a front stagnation point, defined as the location where the shear stress vanishes, is the stabilizing mechanism which turns the ellipse broadside horizontal. Large negative pressures on the back side of the ellipse due to periodic vortex shedding induce the lateral oscillation, but these pressures are relieved after the vortex is shed and the stabilizing mechanism takes over. The viscous stresses oppose the motion, but the resulting torque is an order of magnitude smaller than the pressure torque.

Huang *et al.* (1998) first made the analogy between the unstable vertical orientation of an elliptical cylinder and two 'kissing' circular cylinders. However, they serendipitously discovered a case where an ellipse will settle vertically at a small enough Reynolds number. They corroborated this surprising result with an experiment, and conjectured that the explanation is probably found in lubrication forces at low Reynolds number which would tend to produce high pressures in the converging gap between the walls at the top and bottom of the tilted ellipse. Qi (1999) confirmed this result using a lattice Boltzmann simulation. Huang *et al.* (1998) also performed simulations of sedimentation in a non-Newtonian fluid where they found stable configurations that were either vertical at the centre or tilted off centre when the visco-elastic effects were able to overcome inertial effects. Swaminathan, Mukundakrishnan & Hu (2006) simulated the sedimentation of a three-dimensional ellipsoidal particle in a Newtonian fluid using the finite-element method and showed that for Reynolds numbers of  $O(1)$ , the particle can sediment with an inclination to the horizontal. Aidun *et al.* (1998) simulated multiple elliptical particles settling in a vertical channel with the same configuration while changing the Reynolds number and found the behaviour of the trajectories to change with increasing Reynolds number.

The main focus of this work is to present a detailed investigation of the effects of boundaries on the mode of sedimentation. Previous investigations of sedimentation have mostly considered the case of wide channels (or tubes) where the characteristic size of the channel is at least four times the major axis of the ellipse. As a first step towards understanding the boundary effects, we present here the results of sedimentation of a two-dimensional elliptical particle in narrow channels. Two-dimensional simulations serve as a convenient starting point towards three-dimensional simulations. This is especially true for the LBM, where modifying a two-dimensional code to handle three dimensions is a relatively straightforward task. Further, two-dimensional simulations also help us to understand the effect of dimensionality when the results are compared with those obtained with three-dimensional simulations. In this paper, we will see that the influence of the channel walls on the behaviour of the ellipse extends beyond that which has been previously reported. Even for situations in a Newtonian fluid where the system has sufficient inertia, the presence of the walls can cause the ellipse to behave unexpectedly. For a given system defined by the aspect ratio, density ratio and Reynolds number in a regime prior to vortex shedding, the elliptical particle may pass through several

behavioural regimes for a decreasing blockage ratio: (a) major axis horizontal at the channel centre; (b) inclined off centre; (c) vertical at the channel centre; (d) periodic tumbling and (e) an oscillating mode of sedimentation. Furthermore, we find that for blockage ratios slightly greater than unity, the ellipse develops a seemingly whimsical nature where it will adopt a different regime behaviour for the same blockage ratio, depending on the initial lateral position and orientation. This may prove that other modes of settling depend on more than just the Reynolds number. For the conclusions presented in this paper, the results from the LBM and the finite-element method are consistent.

To perform these simulations more accurately, we augmented Ladd's technique with several enhancements. We adopted the method by Aidun *et al.* (Aidun & Lu 1995; Aidun *et al.* 1998) to remove fluid on the inside of the particle; Mei *et al.*'s (Mei, Luo & Shyy 1999) method to achieve second-order accuracy for boundary conditions on the surface of the particle; Inamuro *et al.*'s (Inamuro, Maeba & Ogino 2000) method to calculate the force on the particle, adapted by Li *et al.* (2004b); Glowinski *et al.*'s (Glowinski *et al.* 2001) method to apply an appropriate lubrication force when there are no fluid nodes between the particle and the sidewall and Yu *et al.*'s (Yu, Mei & Shyy 2002) multi-block method to increase the resolution in the vicinity of the particle. The details of the numerical method are illustrated in §2. The code is validated in §3, and some results for varying aspect ratio and density ratio are given for wide channel sedimentation. Section 4 discusses results for sedimentation in a narrow channel. Finally, some concluding remarks are considered in §5.

## 2. Numerical method

### 2.1. Lattice Boltzmann model

The Lattice Boltzmann Equation (LBE) (Frisch *et al.* 1987; McNamara & Zanetti 1988; Chen, Chen & Matthaeus 1992; Chen & Doolen 1998; Yu *et al.* 2003) with the single relaxation time (SRT) approximation (Bhatnagar, Gross & Krook 1954; Chen *et al.* 1992; Qian, d'Humieres & Lallemand 1992) is written as

$$f_\alpha(\mathbf{x} + \mathbf{e}_\alpha \delta t, t + \delta t) = f_\alpha(\mathbf{x}, t) - \frac{\delta t}{\tau} [f_\alpha(\mathbf{x}, t) - f_\alpha^{(eq)}(\mathbf{x}, t)], \quad (2.1)$$

where  $\tau$  is the relaxation time,  $\mathbf{x}$  is a discretized point in physical space,  $t$  is the discretized time and  $\delta t$  is the time step.  $f_\alpha$  and  $f_\alpha^{(eq)}$  are the distribution function and corresponding equilibrium distribution function associated with the  $\alpha$ th discrete velocity direction  $\mathbf{e}_\alpha$ , respectively. In the two-dimensional nine-velocity lattice (D2Q9) model (Qian *et al.* 1992) shown in figure 1, the discrete velocity set is

$$\mathbf{e}_\alpha = \begin{cases} (0, 0), & \text{for } \alpha = 0 \\ c(\cos((\alpha - 1)\pi/2), \sin((\alpha - 1)\pi/2)), & \text{for } \alpha = 1-4 \\ \sqrt{2}c(\cos((2\alpha - 1)\pi/4), \sin((2\alpha - 1)\pi/4)) & \text{for } \alpha = 5-8. \end{cases} \quad (2.2)$$

Here, the lattice speed  $c = \delta x / \delta t$ , where  $\delta x$  is the lattice constant. The equilibrium distribution functions for this lattice are of the form

$$f_\alpha^{(eq)} = \rho w_\alpha \left[ 1 + \frac{3}{c^2} \mathbf{e}_\alpha \cdot \mathbf{u} + \frac{9}{2c^4} (\mathbf{e}_\alpha \cdot \mathbf{u})^2 - \frac{3}{2c^2} u^2 \right], \quad (2.3)$$

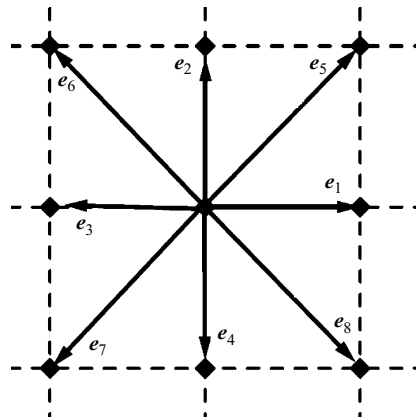


FIGURE 1. Lattice structure of the two-dimensional ‘D2Q9’ lattice.

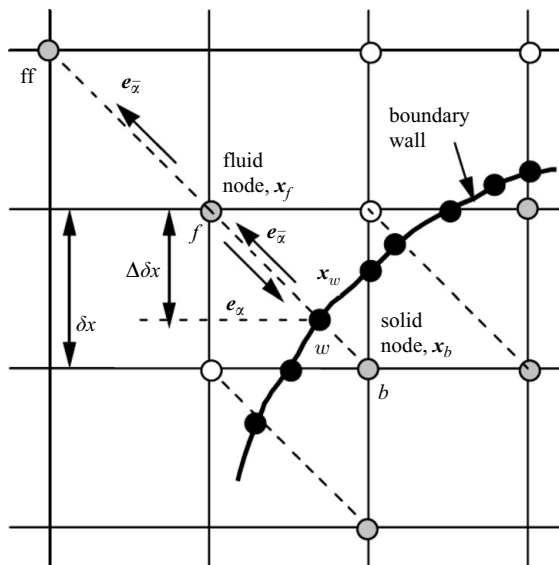


FIGURE 2. A curved wall solid boundary in a two-dimensional lattice –  $x_f$  are the fluid nodes,  $x_b$  are the solid nodes (inside the particle) and  $x_w$  are the locations on the wall where the lattice vectors intersect the solid boundary (from Yu *et al.* 2003).

where  $\rho$  is the fluid density,  $\mathbf{u}$  is the fluid velocity and  $w_\alpha$  are the quadrature weights given by

$$w_\alpha = \begin{cases} 4/9 & \text{for } \alpha=0, \\ 1/9 & \text{for } \alpha=1-4, \\ 1/36 & \text{for } \alpha=5-8. \end{cases} \quad (2.4)$$

The macroscopic Navier–Stokes equations can be obtained from the LBE through a Chapman–Enskog expansion (He & Luo 1997; Chen & Doolen 1998).

### 2.2. Boundary conditions for complex geometry

Consider the solid wall that is represented in figure 2. The particle is mapped onto the existing mesh and the boundary divides the solid region  $x_b$  from the fluid region  $x_f$ . In his simulations of suspension flows, Ladd (1994*b*) placed the wall along the link,

half-way between the fluid and boundary node, referred to as Bounce-Back on the Link (BBL). This portrays the curved boundary as a series of steps and, under certain circumstances, results in spurious oscillations in the vicinity of the boundary (Yu *et al.* 2003). To achieve the highest possible accuracy, the boundary conditions should account for the exact position of the wall ( $\mathbf{x}_w$ ) along the link. For simulations that involve moving complex boundaries, we employ the method proposed by Filippova & Hanel (1997) and improved upon by Mei *et al.* (1999). Mei *et al.* demonstrated that their scheme is both accurate and stable. Instead of placing the solid wall at the centre of the link, this method explicitly computes the fraction of a link in the fluid domain and uses this information along with an interpolation technique to implement the boundary conditions. The fraction of link in the fluid is computed as

$$\Delta = \frac{|\mathbf{x}_f - \mathbf{x}_w|}{|\mathbf{x}_f - \mathbf{x}_b|}. \quad (2.5)$$

After the streaming operation in the LBM, the distribution function along  $\mathbf{e}_\alpha$  at the wall can be obtained using linear interpolation between the fluid node and the boundary node,

$$f_\alpha(\mathbf{x}_w, t + \delta t) = f_\alpha(\mathbf{x}_f, t + \delta t) + \Delta[f_\alpha(\mathbf{x}_b, t + \delta t) - f_\alpha(\mathbf{x}_f, t + \delta t)]. \quad (2.6)$$

To guarantee the no-slip boundary condition at the wall, the unknown distribution function along  $\mathbf{e}_{\bar{\alpha}}$  can be computed as

$$f_{\bar{\alpha}}(\mathbf{x}_w, t + \delta t) = f_\alpha(\mathbf{x}_w, t + \delta t) + 6w_\alpha\rho_w \frac{\mathbf{e}_\alpha \cdot \mathbf{u}_w}{c^2}, \quad (2.7)$$

where  $\mathbf{u}_w$  is the wall velocity. We can now compute  $f_{\bar{\alpha}}(\mathbf{x}_f, t + \delta t)$  using

$$f_{\bar{\alpha}}(\mathbf{x}_f, t + \delta t) = f_{\bar{\alpha}}(\mathbf{x}_w, t + \delta t) + \frac{\Delta}{1 + \Delta}(f_{\bar{\alpha}}(\mathbf{x}_f + \mathbf{e}_{\bar{\alpha}}, t + \delta t) - f_{\bar{\alpha}}(\mathbf{x}_w, t + \delta t)). \quad (2.8)$$

Due to the movement of solid particles over the lattice, certain nodes which were in the fluid domain at one time step may be covered by the particle the subsequent time step. The fluid at this node is removed from the system (Aidun & Lu 1995; Aidun *et al.* 1998). On the other hand, a node may be in the solid region at a particular time step, and on the ensuing time step find itself in the fluid region. When such a fluid node is recovered, the distribution function at this newly created node is assumed to be the average of the extrapolated distribution function values from a *second-order extrapolation scheme* over all the possible directions (Chen, Martinez & Mei 1996; Fang & Chen 2004). Fang *et al.* (2002) has shown that the mass is approximately conserved at the boundaries.

### 2.3. Force calculation on particle surface

The calculation of the hydrodynamic force and torque on a solid particle immersed in a fluid flow is a matter of critical importance. Since the behaviour of the particle and the carrier fluid are directly coupled, the obligation to incorporate an accurate force calculation algorithm is evident.

#### 2.3.1. Stress integration

The two methods of force calculation used in the LBM are the momentum exchange (ME) method (Ladd 1994*a, b*; Aidun *et al.* 1998; Mei *et al.* 2002), unique to the LBM, and the method of stress integration (SI) (He, Luo & Dembo 1996; He & Doolen 1997; Filippova & Hanel 1998). While the ME method has its advantages, we adopt

the SI method for this work because it is accurate, and easily implemented in two dimensions. The force on the particle due to the fluid is given by,

$$\mathbf{F} = \int_{\partial\Omega} \boldsymbol{\sigma} \cdot \mathbf{n} dS, \tag{2.9}$$

where  $\boldsymbol{\sigma}$  is the stress tensor,  $\partial\Omega$  is the surface of the particle,  $\mathbf{n}$  is the outward pointing normal vector and the integration is on the surface of the particle. The stress tensor is given by,

$$\sigma_{ij} = -p\delta_{ij} + 2\mu S_{ij}, \tag{2.10}$$

where  $p$  is the pressure and

$$S_{ij} = \frac{1}{2} \left( \frac{\partial u_i}{\partial x_j} + \frac{\partial u_j}{\partial x_i} \right). \tag{2.11}$$

One of the advantages of the LBE is that the viscous stresses can be computed using the non-equilibrium components of the distribution function (Mei *et al.* 2002). Inamuro *et al.* (2000) showed that the stress tensor can be calculated using

$$\sigma_{ij} = -\frac{1}{2\tau} p\delta_{ij} - \frac{\tau - 1/2}{\tau} \sum_{\alpha} f_{\alpha} (e_{\alpha i} - u_i)(e_{\alpha j} - u_j). \tag{2.12}$$

Li *et al.* (2004*b*) used (2.12) to determine the stress tensor on the surface of the particle after suitably extrapolating the distribution functions to the wall. The force and torque on the surface are calculated by integrating the extrapolated stress tensor over the particle surface, where the integral is approximated by the quadrature of 400 points. After the force and torque on the particle are determined, the translation and rotation of the particle are updated at each Newtonian dynamics time step, by using a half-step ‘leap-frog’ scheme (Allen & Tildesley 1987; Li *et al.* 2004*b*).

### 2.3.2. Particle–wall interaction

Due to the fact that our simulations involve narrow channels, the particle will inevitably travel close to the wall under certain circumstances. When the particle wanders so close that there are no fluid nodes on the fixed grid between the particle surface and the wall, the above force calculation will break down at that point. If the gap between the particle and the wall is less than some threshold distance, in this case a single lattice unit, a supplementary short-range repulsive force should be introduced to prevent the particle from penetrating the wall. There are two different ways to get this repulsive force. One is to add a spring force (Höfler & Schwarzer 2000; Glowinski *et al.* 2001; Feng & Michaelides 2004). Since their formula is for circular case, we have adjusted it slightly to account for elliptical particles. The repulsion force is given as

$$F_R = \begin{cases} 0, & |\mathbf{x} - \mathbf{x}_c| > \zeta \\ \frac{C}{\varepsilon_w} \left( \frac{1}{\zeta} \right)^2 (|\mathbf{x} - \mathbf{x}_c| - \zeta)^2 (|\mathbf{x} - \mathbf{x}_c|/|\mathbf{x} - \mathbf{x}_c|), & |\mathbf{x} - \mathbf{x}_c| \leq \zeta. \end{cases} \tag{2.13}$$

Here,  $\mathbf{x}_c$  is the point on the elliptical particle closest to the wall, and  $\mathbf{x}$  is the corresponding point on the wall, i.e.  $|\mathbf{x} - \mathbf{x}_c|$  is the smallest distance between any point on the ellipse and the wall.  $C$  is a force scale and  $\varepsilon_w$  is a stiffness parameter to be determined.  $\zeta$  is the threshold distance mentioned above.  $C = (\rho_p - \rho_f)A_p g$  is the relative gravitational force scale, where  $\rho_p$  and  $\rho_f$  are the solid and fluid density, respectively,  $A_p$  is the area of the ellipse and  $g$  is the gravitational acceleration. Unlike



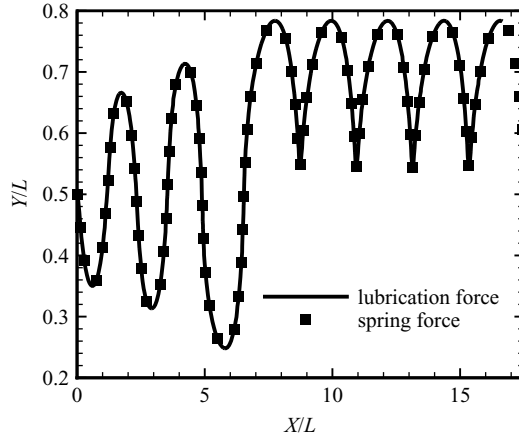


FIGURE 3. Comparison of the trajectories of an elliptical particle when the particle–wall interaction is important. The solid line is for the lubrication force correction and the solid squares are for the spring force correction. The parameters (defined in §3) for this simulation are aspect ratio  $\alpha = 2.0$ , blockage ratio  $\beta = 16/13$  and density ratio  $\gamma = 1.1$ .

the circular particle case, this force produces a torque for an elliptical particle as it is not necessarily directed through the centre of mass.

Another approach is to introduce a lubrication force (Ladd 1994 *b*; Ladd & Verberg 2001; Nguyen & Ladd 2002; Li *et al.* 2004*a*). The lubrication formula for two circular cylinders is as follows:

$$F_L = \begin{cases} 0, & \lambda > \zeta \\ -\frac{3}{2}\pi\mu \left[ \frac{2R_a R_b}{R_a + R_b} \left( \frac{1}{\lambda} - \frac{1}{\zeta} \right) \right]^{3/2} (v_a^N - v_b^N) \frac{\mathbf{x}_a - \mathbf{x}_b}{|\mathbf{x}_a - \mathbf{x}_b|}, & \lambda \leq \zeta, \end{cases} \quad (2.14)$$

where  $\mu$  is the fluid viscosity,  $R_a$  and  $R_b$  are the radii of the cylinders,  $v_a^N$  and  $v_b^N$  are their velocities along the line joining their centres and  $\lambda$  is the gap between the cylinders. Also, the same adjustment should be made to account for elliptic particle. In figure 3, we compare the trajectory of an elliptical particle computed using two different repulsive force approximations. The solid curve was obtained using the lubrication correction and the symbols were obtained using spring force correction. It can be seen that the repulsive force schemes do not alter the dynamics of the particle. For the results shown in this paper, the spring force scheme is used, where  $\varepsilon_w = 0.25$  and  $\zeta = 1.0$ . The results were also found to be consistent with those obtained with a finite-element method in which the mesh is adaptive and locally fine enough to resolve the gap between the particle and the wall. No lubrication method is used for the finite-element model.

#### 2.4. Dynamic multi-block scheme

In order to improve the simulation accuracy without rendering the computational cost prohibitive, we refined the mesh in the vicinity of the particle using a multi-block scheme. Our scheme is essentially the same as the multi-block scheme presented by Yu *et al.* (2002), the only difference being that the refined grid travels with the particle. The refinement is applied over a subdomain the entire width of the channel, a length of one particle major-axis ahead through one and a half major-axis behind the centre of mass in the vertical direction. Given the particle position at a particular



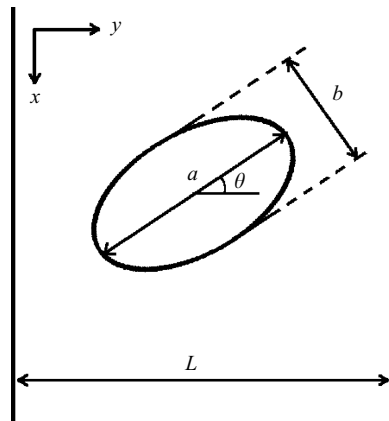


FIGURE 4. The geometry of the simulation domain –  $a$  and  $b$  are the major and minor axes of the particle,  $\theta$  is the orientation of the particle with the horizontal.

time step, we refine the subdomain as if the particle were static. Then every time the particle progresses one vertical lattice unit in the coarse grid, the refined subdomain gets shifted, in essence adding one ‘layer’ ahead of the particle and removing one ‘layer’ behind. The refinement factor defines the size of the ‘layer’ of fine lattice units corresponding to one coarse lattice unit. We perform simulations using refinement factors as large as four.

### 2.5. Finite-element computations

To verify the results from the lattice Boltzmann computations, we also performed a set of simulations using the finite-element method. The method, originally developed by Hu *et al.* (1992), uses an Arbitrary Lagrangian–Eulerian (ALE) formulation with a moving finite-element mesh. A recent review of the method along with several benchmark problems are reported in Hu, Patankar & Zhu (2001). The ALE method uses a six-node curved element spacial discretization with a second-order discretization in time. The method combines an explicit update of the finite-element mesh and the particle position with an implicit calculation of the fluid and particle velocities for enhanced numerical stability. Compared to the lattice Boltzmann technique, this method has the advantage of being able to simulate the dynamics of particulate systems without resorting to an artificial lubrication force – when the particle gets too close to a wall, the mesh automatically improves its resolution locally to resolve the gap between the particle and the wall. However, the disadvantage with such an approach is that, as the mesh moves along with the particle it tends to get distorted or elongated and the mesh needs to be regenerated periodically. This is in general a computationally expensive operation.

## 3. Validation of the numerical method

A schematic illustration of the computational domain for this work is shown in figure 4. The major and minor axes of the ellipse are  $a$  and  $b$ , respectively, the width of the domain is  $L$  and the particle’s angle of inclination with respect to the horizontal axis is  $\theta$ . Choosing the major axis of the particle as the length scale, we see that there

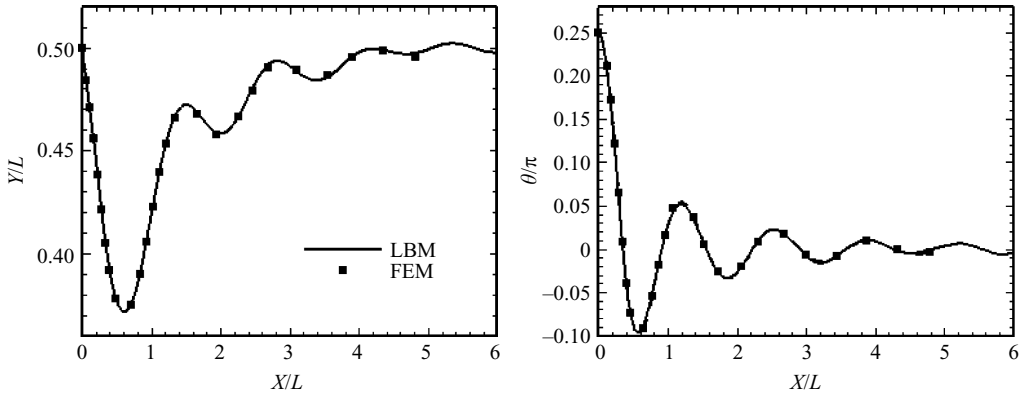


FIGURE 5. Comparison of particle trajectories (location of centre of mass at different times) and orientations obtained from LBM and FEM. The parameters for the case are  $\alpha = 2.0$ ,  $\beta = 4.0$  and  $\gamma = 1.1$ .

are four dimensionless parameters given by

Aspect ratio	$\alpha = a/b,$
Blockage ratio	$\beta = L/a,$
Density ratio	$\gamma = \rho_p/\rho_f,$
Terminal Reynolds number	$Re = U_t a/\nu,$

where  $\rho_p$  and  $\rho_f$  are the densities of the particle and the fluid respectively,  $U_t$  is the terminal velocity of the particle and  $\nu$  is the viscosity of the fluid. In physical units, the major axis of the ellipse is 0.1 cm and the kinematic viscosity of the fluid is taken to be  $0.01 \text{ cm}^2 \text{ s}^{-1}$ . The lattice Boltzmann simulations use a coarse grid with a resolution of 260 grid cells per cm. For narrow channel simulations where the wall effects are crucial, we used a refinement factor of 4 in the vicinity of the particle. This gives a fine-grid resolution of 104 grid cells across the major axis. The coarse-grid relaxation time ( $\tau_c$ ) is equal to 0.6, which gives about  $2 \times 10^4$  coarse-grid time steps per second.

In figure 5, we compare the results of the particle’s trajectory (location of the centre of mass at different times) computed using the LBE and the finite-element method when  $\beta = 4.0$  and  $\alpha = 2.0$ . The density ratio is  $\gamma = 1.1$  and the particle is started in the centre of the domain with an initial angle of  $\theta_0 = \pi/4$ . It is clear that the results obtained using both the methods are extremely consistent with each other. The particle settles in the centre of the channel and sediments in a horizontal configuration ( $\theta = 0$ ).

In figure 6 we show the streamlines across the fine mesh – coarse mesh boundary. It can be seen that the flow proceeds smoothly between the domains with different resolution, and there are no oscillations due to the multi-block scheme. We also performed some simulations where the size of the fine-grid domain was changed. A simulation using fine grid everywhere gave the same results as the one with multi-block implementation. The local multi-block scheme permits us to get much better resolution closer to the particle and is especially useful when the particle is very close to the walls.

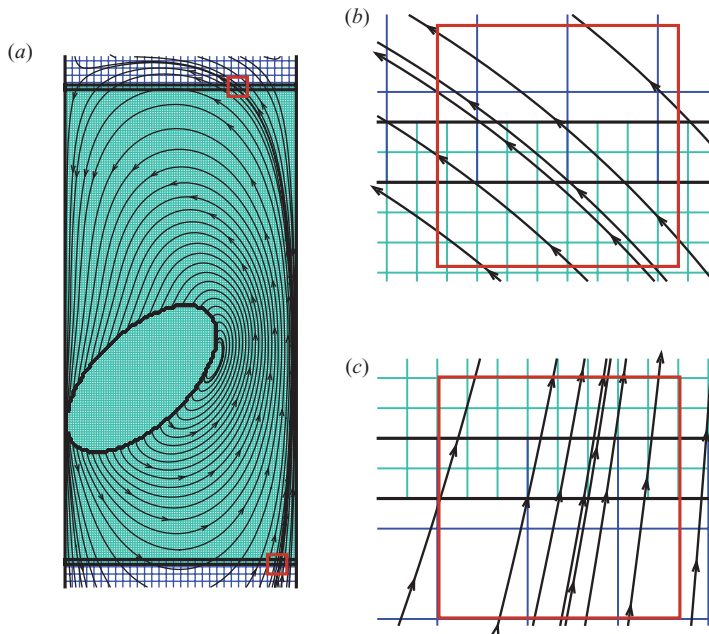


FIGURE 6. (a) Streamlines across the coarse mesh – fine mesh boundary. Also shown are views of the streamlines magnified by a factor of 25 (b) behind the particle and (c) ahead of the particle.

### 3.1. Effect of density ratio

In this section, we describe the pattern of sedimentation when the density ratio varied in the range  $1.01 \leq \gamma \leq 2.5$ . For boundary conditions in the direction of gravity, we impose a no-flow condition ( $\mathbf{v} = 0$ ) at a distance of  $10a$  ahead of the particle, where  $a$  is the major axis. Behind the particle, the flow is taken to be fully developed at a distance of  $15a$  when the density ratio  $\gamma \leq 1.15$ . For higher density ratios, the particle periodically sheds vortices and we need to use a larger domain size. The fully developed flow condition is applied  $25a$  behind the particle when  $1.15 < \gamma \leq 1.5$  and  $40a$  behind the particle when  $\gamma > 1.5$ . To check the accuracy of these boundary conditions, we have also performed simulations with a closed domain (walls on all four sides) with a total length of  $100a$ . Figure 7 shows the terminal Reynolds number as a function of the density ratio. These simulations were performed with a blockage ratio of  $\beta = 4.0$  and with elliptical particles of aspect ratio  $\alpha = 2.0$ . The particles were released from the centre of the domain with an initial inclination of  $\theta = \pi/4$  to break the symmetry. In cases where the final state of the particle is of an oscillating nature, the Reynolds number was calculated using the average velocity. For low density ratios ( $\gamma - 1 \ll 1$ ), the nonlinear terms are negligible and the flow is dominated by viscous effects. This results in a linear increase of the terminal velocity with the density ratio. For higher density ratios ( $\gamma - 1 \sim O(1)$ ), the drag on the particle becomes quadratic in the mean velocity, resulting in the Reynolds number scaling as

$$Re \sim \left( \frac{\Delta\rho}{\rho_f} \right)^{0.5} = (\gamma - 1)^{0.5}. \quad (3.1)$$

The density ratio also effects the mode of sedimentation. For low density ratios, the particle sediments horizontally with a constant velocity, whereas for higher density

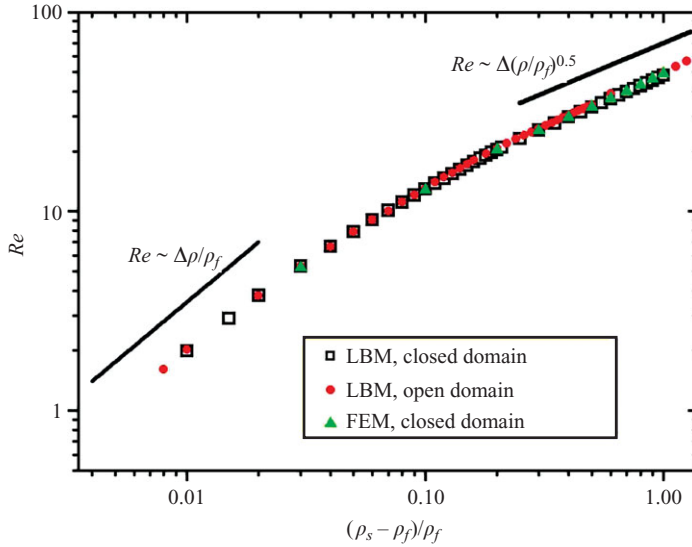


FIGURE 7. Terminal Reynolds number as a function of the density ratio with  $\beta = 4.0$  and  $\alpha = 2.0$ .

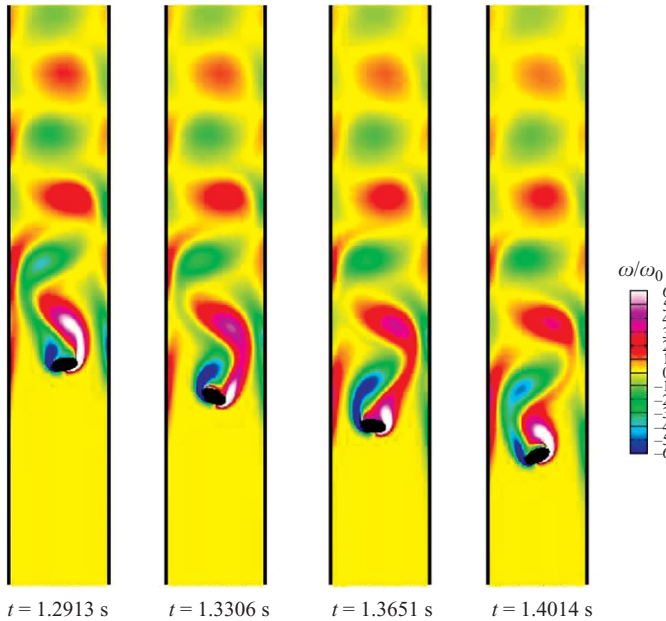


FIGURE 8. Contours of vorticity during oscillatory sedimentation of an elliptical particle with  $\alpha = 2.0$ ,  $\beta = 4.0$ ,  $\gamma = 1.5$  and  $\omega_0 = v/a^2$ .

ratios we observe an oscillating pattern due to the periodic shedding of vortices behind the particle. The flow patterns during this oscillating phase are shown in figure 8 and the transition between the two regimes is shown in figures 9 and 10.

### 3.2. Effect of aspect ratio

We now investigate the effect of varying the particle aspect ratio. Here we used multi-block scheme with a refinement factor of 3. The aspect ratio is varied between

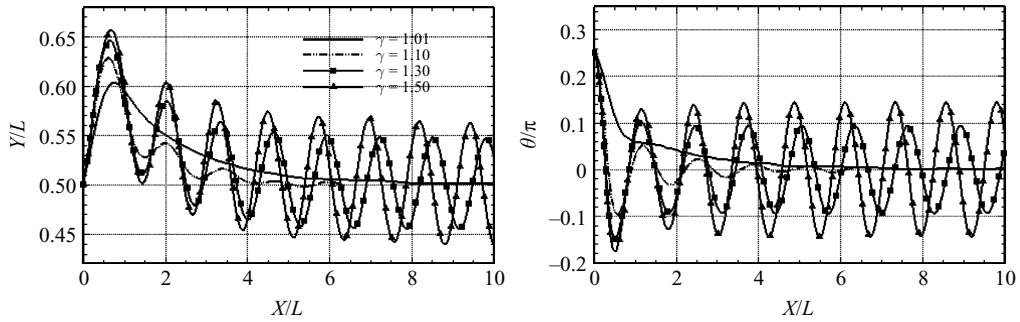


FIGURE 9. Pattern of sedimentation for different density ratios with  $\beta = 4.0$  and  $\alpha = 2.0$ . For low density ratios ( $\gamma = 1.01$  and  $1.1$ ) the particle settles down with a constant velocity. For higher density ratios ( $\gamma = 1.3$  and  $1.5$ ) the particle sediments with an oscillatory motion.

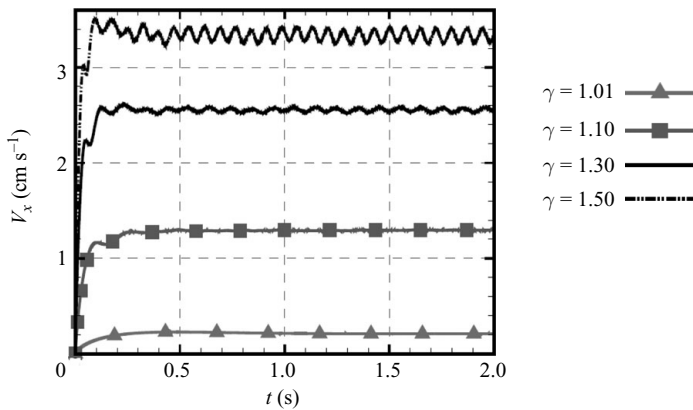


FIGURE 10. The vertical velocities of sedimentation for different density ratios (corresponding to the cases shown in figure 9).

$\alpha = 1$  (corresponding to a circular particle) and  $\alpha = 13$ . In all of these simulations, the blockage ratio is fixed at  $\beta = 4.0$ . The major axis of the particle is also held fixed. For the most slender shape, the minor axis was resolved using six lattice units. In figure 11, we show the terminal Reynolds number for different aspect ratios. The Reynolds number is seen to display a non-trivial scaling with the aspect ratio as

$$Re \sim \alpha^{-0.7}. \quad (3.2)$$

It must be noted that there are two different effects that are responsible for this scaling: (i) change in the aspect ratio and (ii) change in the mass of the particle. To keep all the non-dimensional parameters except the aspect ratio fixed, the density ratio was also kept constant. This results in the mass of the particle reducing with increasing aspect ratio. However, we find that the exponent of  $-0.7$  cannot be explained using any simple argument and further careful study is needed to explain this dependence.

#### 4. Results for narrow channels

For sufficiently large blockage ratio the sedimentation pattern naturally becomes independent of the size of the domain. In the case of  $\gamma = 1.1$ , when the blockage ratio  $\beta$  is larger than  $2.0$ , the particle always settles horizontally with a constant terminal

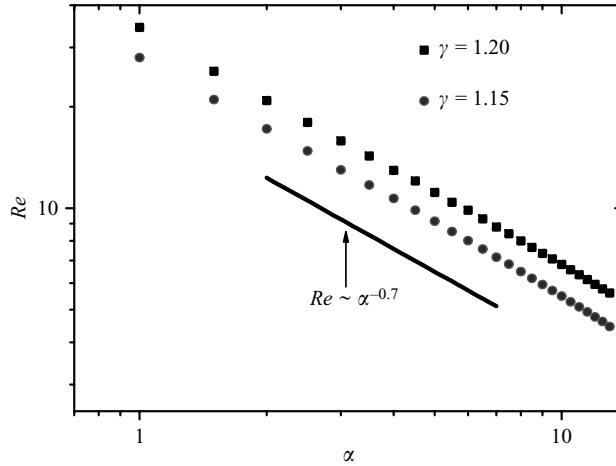


FIGURE 11. Terminal Reynolds number as a function of the aspect ratio with  $\beta = 4.0$  and  $a = 26$ . In cases where the particle oscillates, the average velocity is used.

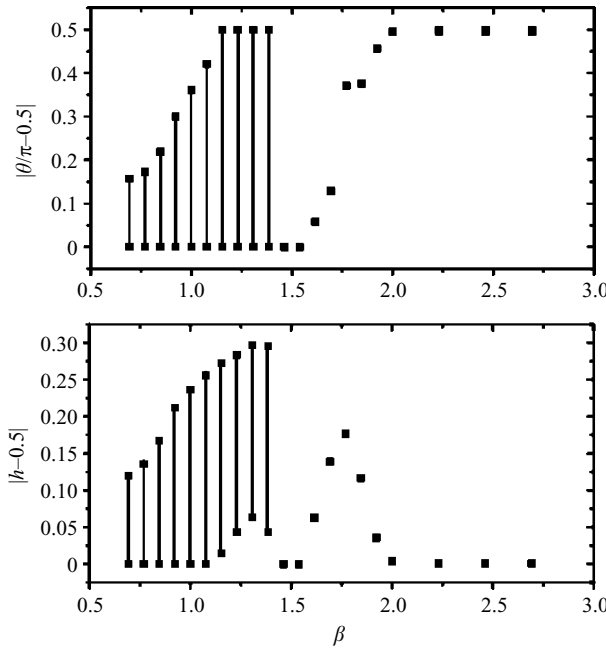


FIGURE 12. Terminal state orientation and position of the particle for different blockage ratios with  $\gamma = 1.1$  and  $\alpha = 2.0$ . Cases where the particle is oscillating ( $\max\{|\theta/\pi - 0.5|\} < 0.5$ ,  $\beta < 2.0$ ) or tumbling ( $\max\{|\theta/\pi - 0.5|\} = 0.5$ ,  $\beta < 2.0$ ) are denoted using lines representing the range of oscillation. Here  $h = y/L$ .

velocity. As the blockage ratio is reduced below 2.0, the system begins to transit into different kinds of sedimentation. For this case, we also show in this section that the pattern of sedimentation depends sensitively on the initial conditions.

In figure 12, we show the terminal state orientation  $\theta$  and horizontal positions  $h = y/L$  of the particle for different blockage ratios. We also present snapshots of the particle's position in different modes of sedimentation in figure 13. For extremely

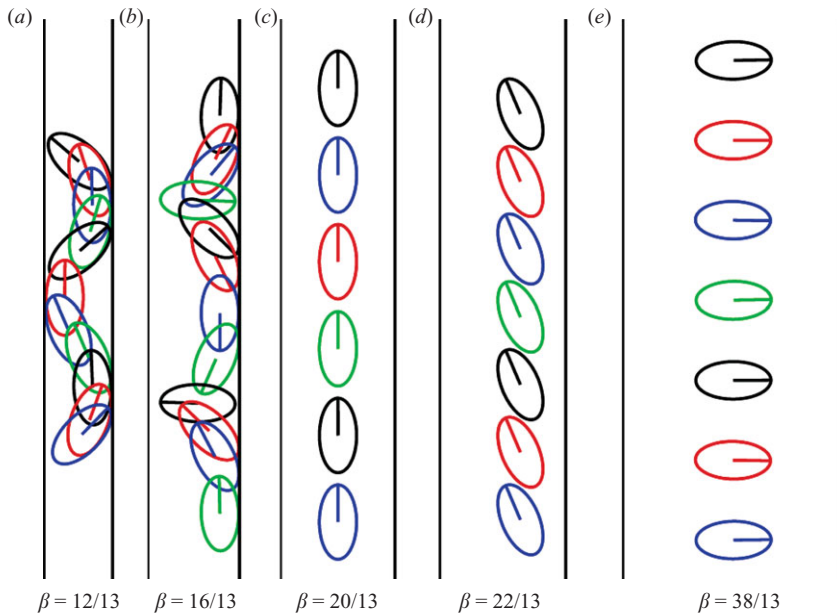


FIGURE 13. Snapshots of five different patterns with  $\gamma = 1.1$ ,  $\alpha = 2.0$ , initial angle  $\theta_0 = \pi/3$  and initial positions  $y = 0.5L$ . Colour is added for visual clarity only.

low blockage ratios where the width of the channel is smaller than the major axis of the particle ( $\beta \leq 1.0$ ), the particle ‘wiggles’ down the channel, oscillating around the centreline. This is represented in figure 12 with lines that show the magnitude of the particle’s oscillation. Snapshots of this oscillatory motion as observed in an LBM simulation ( $\alpha = 2.0$ ,  $\beta = 12/13$  and  $\gamma = 1.1$ ) are shown in figure 13(a). As the blockage ratio is slowly increased, the magnitude of the oscillation also increases. Eventually the oscillations transition to a ‘tumbling regime’ where the particle rolls down along one of the walls of the channel. This is represented in the plot with lines spanning the entire range  $[0, \pi]$ . This tumbling motion which is sketched in figure 13(b) is seen to be associated with an anomalous rotation as reported for circular particles by Liu *et al.* (1993), Feng *et al.* (1994a) and Hu (1995).

A further increase in the blockage ratio results in the particle sedimenting vertically (shown in figure 13c) for a small range of blockage ratios ( $\beta \sim 1.5$ ). This mode of sedimentation is only observed for a very narrow range of blockage ratios. It must be mentioned that the Reynolds number for this simulation is  $O(10)$  as opposed to the vertical sedimentation observed by Huang *et al.* (1998) where the blockage ratio was  $\beta = 5.0$  and the Reynolds number was much lower ( $Re = 0.31$ ). In the results published in Huang *et al.* (1998), the vertical sedimentation is a low-Reynolds-number effect, whereas, in our simulations the vertical sedimentation occurs due to the strong effect of the boundaries. When  $1.5 \leq \beta \leq 2.0$ , the particle sediments off-centre with a constant non-trivial inclination to the horizontal. This inclined sedimentation is sketched in figure 13(d). A similar inclined mode of sedimentation was observed for three-dimensional ellipsoids sedimenting in infinitely long tubes by Swaminathan *et al.* (2006). In this work, the particle is sedimenting in a relatively wide tube (diameter is four major axes) and the inclined mode is seen to occur for Reynolds number of  $O(1)$ . The orientation of the particle at steady state was found to vary between  $82^\circ$  and  $90^\circ$ . However, the inclined mode shown in this paper is the result of extremely



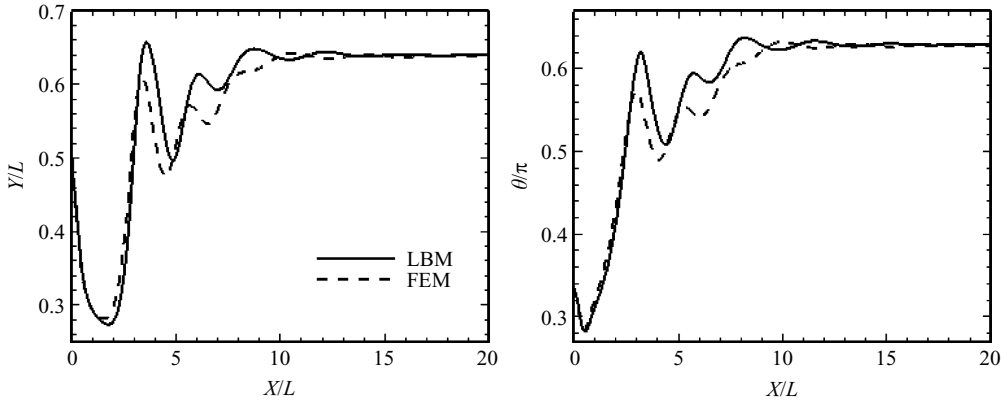


FIGURE 14. Trajectory of the particle computed using LBM and FEM. Both the methods show the particle to be sedimenting with an inclination to the horizontal. The parameters for this simulation are  $\alpha = 2.0$ ,  $\beta = 22/13$  and  $\gamma = 1.1$ .

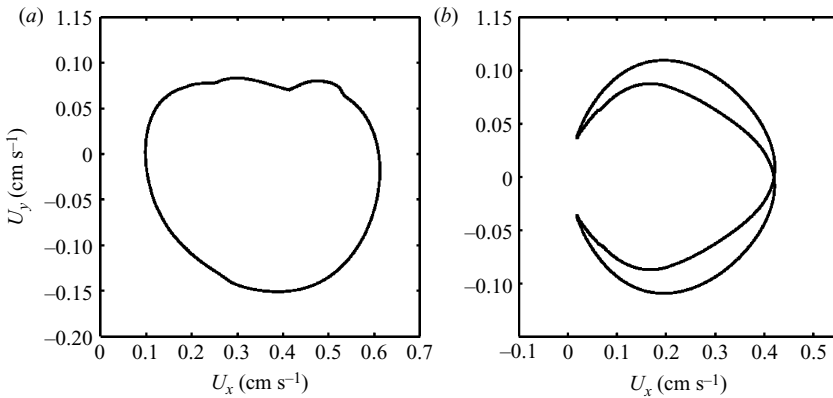


FIGURE 15. Trajectory of the steady-state velocities for different modes of sedimentation (a) Tumbling mode with  $\beta = 17/13$ ,  $\alpha = 2.0$  and  $\gamma = 1.1$  and (b) Oscillatory mode with  $\beta = 1.0$ ,  $\alpha = 2.0$  and  $\gamma = 1.1$ .

strong wall effects and the inclination of the ellipse varies smoothly from  $0^\circ$  to  $90^\circ$  forming a bridge between the vertical and horizontal modes of sedimentation. The Reynolds numbers obtained in our work are also higher by an order of magnitude – for the case shown in figure 14, we have  $Re = 8.7$ . An inclined mode of sedimentation was also reported by Huang *et al.* (1998) for sedimentation of elliptical particles in Oldroyd-B fluids. The angle which the particle makes with the horizontal decreases monotonically until  $\beta = 2.0$  beyond which the particle always sediments horizontally. To verify that this result is not a numerical artefact, we compared the results of the LBM computation with those obtained using a finite-element computation using the same initial conditions. In figure 14, we show the trajectory of the particle obtained using the two different methods. While there is some difference in the transient dynamics of the particle, both simulations terminate with a steady state in which the particle is sedimenting slightly off-centre with an inclination of  $\theta \sim 0.63\pi$ .

In figure 15, we show the steady-state velocity of the particle in a  $U_x$  versus  $U_y$  plot. The horizontal, inclined and vertical modes of sedimentation are fixed points on

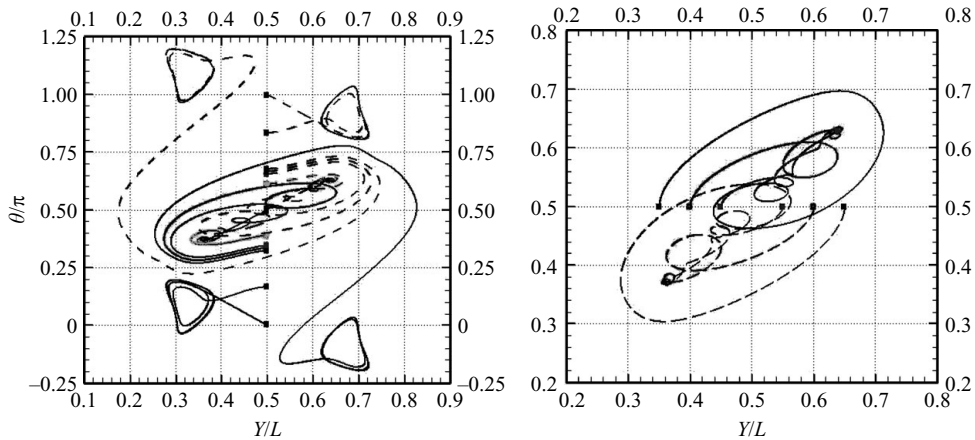


FIGURE 16. Trajectories of the particle for simulations with (a) different initial angles of orientation, all released from the centre of the channel and (b) different initial lateral positions, all started from a vertical configuration. In these cases,  $\alpha = 2.0$ ,  $\beta = 22/13$  and  $\gamma = 1.1$ .

such a representation and are not shown in figure 15. For lower blockage ratios, there is a Hopf bifurcation to a tumbling state along one wall which is shown as the orbit in figure 15(a). At even lower blockage ratios, we get a wall-to-wall oscillation which appears as the two-period orbit as shown in figure 15(b). A detailed investigation of this kind was performed by Aidun & Ding (2003) for a two-cylinder system showing the period-doubling transition to chaos.

In summary, there are a total of five sedimentation patterns which are realized: (i) oscillating (figure 13a), (ii) tumbling (figure 13b), (iii) vertical sedimentation (figure 13c), (iv) inclined sedimentation (figure 13d) and (v) horizontal sedimentation (figure 13e) for these cases the parameters are  $\gamma = 1.1$ ,  $\alpha = 2.0$ ,  $h_0 = 0.5$  and  $\theta_0 = \pi/3$ .

For blockage ratios less than unity, the lack of space restricts the motion of the particle to that of oscillation. When  $1.5 \leq \beta \leq 2.0$  however, the particle has more possibilities and the steady-state pattern depends sensitively on the initial conditions. In figure 16, we plot the trajectory of the particle starting from multiple initial conditions. The initial conditions are marked by the bold squares. In figure 16(a), we show the trajectories when the particle is released from the centre of the channel with different initial angles of orientation. The plot is symmetric about  $\theta = \pi/2$  as one would expect. For small initial angles of inclination, the particle glides along its major axis until it gets close to the wall and sediments executing an oscillatory motion along the wall. In figure 16(a) this is represented by the periodic orbits in the bottom-left and top-right of the diagram. When  $\theta \in (0, \pi/4)$  the oscillation is along the left wall and for  $\theta \in (3\pi/4, \pi)$  the oscillation is along the right wall. For  $|\theta - \pi/2| < \pi/6$ , the particle sediments making a constant angle with the horizontal. This mode of sedimentation is shown by the set of fixed points in the diagram. For the case shown in figure 16, the fixed points are  $\theta = 0.37\pi$  and  $0.63\pi$ . If the angle of inclination is close to  $\pi/4$ , the particle gets too close to the wall during its gliding motion and encounters a strong interaction force due to the wall. This results in the particle being pushed to the opposite wall and sedimenting along it with an oscillatory motion. This mode of sedimentation is shown by the trajectories starting at  $\theta = 0.3\pi$  and  $0.7\pi$  in figure 16(a). In figure 16(b), we show the effect of varying the initial lateral position of the particle, keeping the initial inclination fixed at  $\theta = \pi/2$ .

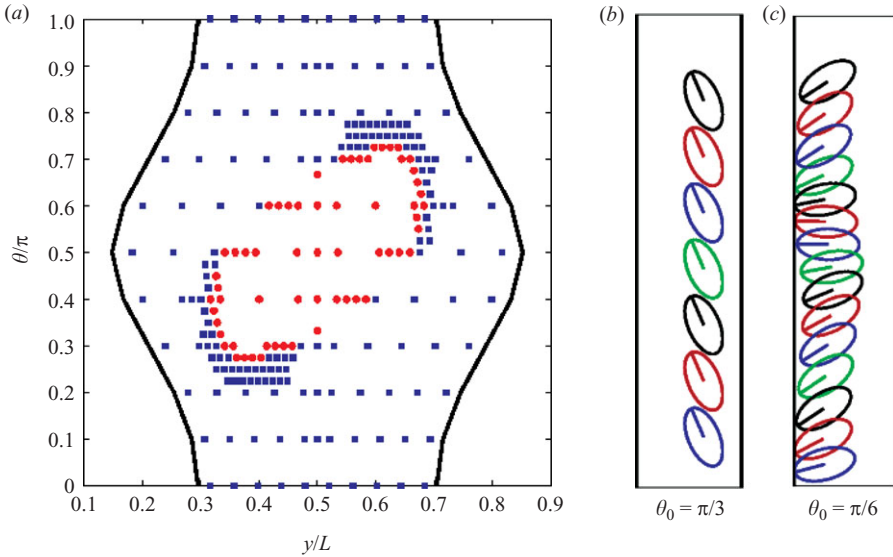


FIGURE 17. Phase space of initial conditions showing regions leading to oscillating sedimentation (blue squares) and the inclined mode of sedimentation (red circles). The solid lines denote the phase-space boundary – for points on this line, the ellipse will make contact with the sidewalls. Also shown are snapshots of the particle executing the two different modes of sedimentation.

We have done a detailed study of the basins of the attraction of the two different modes of sedimentation. In figure 17(a), we show the final mode of sedimentation for a large set of initial conditions. The space of initial conditions is seen to be sharply divided into two distinct regions. In this figure, the blue squares represent the initial conditions leading to an oscillation along one of the walls whereas the red circles represent the inclined mode. The solid black lines represent a geometric constraint reflecting the size of the ellipse – it is not possible for the particle’s centre of mass to be beyond these lines. In figures 17(b) and 17(c) we show the snapshots of the particle’s position during the inclined mode and the oscillatory mode, respectively. During the oscillation along the wall, we notice that the particle briefly executes a pivoting motion when it is closest to the wall. In the periodic orbits shown in figure 16(a), this corresponds to the point where the orientation of the particle changes sign. This motion is different from the pivoting motion described in Russel *et al.* (1977) and observed by Swaminathan *et al.* (2006) in their simulations. We believe that the pivoting motion described in Russel *et al.* (1977) is a purely three-dimensional effect. In two dimensions, such a motion would require the entire fluid to be squeezed through the narrow gap between the particle and the wall. The flow produces enough torque to make this mode unstable. In three dimensions however, it is possible for the fluid to flow around the particle, maintaining stability of the motion.

#### 4.1. Anomalous rotation near the wall

It has been mentioned that a circular particle sedimenting in a channel rotates as it approaches its equilibrium position. It was previously noted (Feng *et al.* 1994a; Hu 1995) that although the particle translates in the downward vertical direction, it rotates as if it was contacting and rolling up the near wall. This phenomenon is not

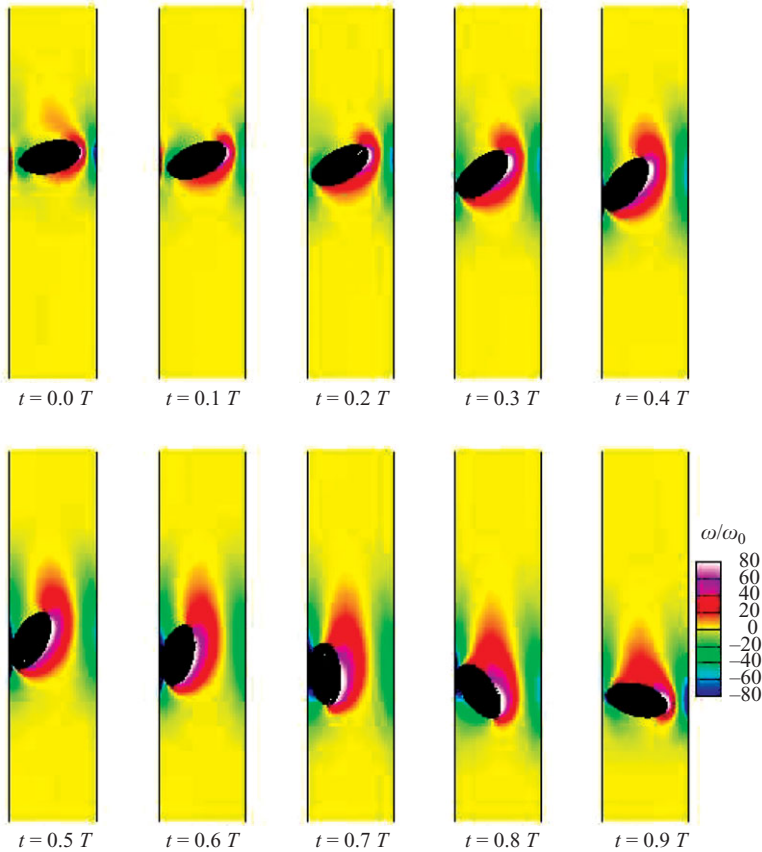


FIGURE 18. Snapshots of a particle ( $\alpha = 2.0$ ) tumbling along the wall – shown are the contours of vorticity. The particle's sense of rotation is as if it was rolling up the wall. The blockage ratio is  $\beta = 1.23$  and density ratio  $\gamma = 1.1$ .

necessarily intuitive and was given the appellation ‘*Anomalous Rotation*’. Hu (1995) performed finite-element simulations to analyse the forces and torques acting on a sedimenting cylinder. He also performed a lubrication analysis when the particle is translating very close to the wall, and concluded that the torque was independent of the gap thickness. It was hypothesized that this behaviour was due to wall effects, but a more specific explanation is yet to be presented. Similarly in our elliptical sedimentation results, for the cases where the particle exhibits a continuous rotation, we find that this rotation is also in the anomalous sense. In figure 18, we show the contours of the fluid vorticity at different instances during one period of the particle's rotation along the wall. The particle executes a tumbling motion with a sense of rotation as if it was moving up the wall.

A definitive explanation of this phenomenon remains elusive because the net torque on the particle is small compared to the individual positive or negative contributions. In figure 19, we show the normal and tangential components of the force on the surface of the particle corresponding to the snapshots in figure 18. At every point, the normal vector is the contribution due to the pressure and the tangential component is due to the shear stress. It can be seen that when the particle configuration is close

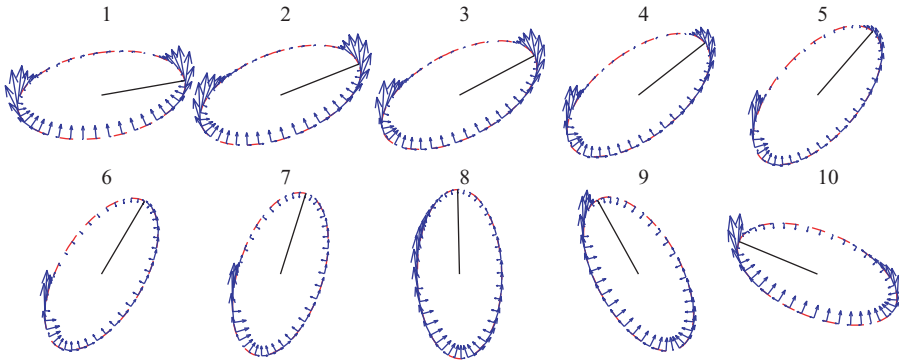


FIGURE 19. Distribution of pressure and viscous forces on a particle tumbling along the wall (not shown, on the left of the particle) for the snapshots shown in figure 18.

to horizontal, the torque due to the flow in the narrow gap between the particle and the wall (on the left) is comparable to that due to the flow on the wider side.

In figure 20(a–e), we show the local torque normalized by  $T_g = (\gamma - 1)\rho_f A_p g a$  (where  $A_p$  is the area of the particle) on the surface of the particle due to the pressure and shear stresses. Unlike circular particles, for an elliptic particle the local normal to the surface does not pass through the centre of the ellipse, except, at the tips of major and minor axes. For this reason, pressure forces also make a contribution to the torque on the particle. It can be seen that the contribution from pressure vanishes at the ends of the major and minor axes, as expected. Also shown in figure 20(f) are the total pressure and viscous contributions to the torque at different instances during the particle's period of oscillation. The fact that the angular velocity is periodic requires that the time-integral of the total torque over a period vanishes, which is seen to be the case from the LBM simulations.

The distributions of torque offer us some insight into the dynamics of the anomalous rotation. When the particle is released with some inclination, it glides along its major axis until it gets close to the wall. Throughout this discussion, we will assume that the initial inclination is  $\theta < \pi/2$  such that the motion of the particle is towards the left wall. During this motion, the shear stress due to the fluid being displaced upwards tends to rotate the particle in the anticlockwise sense whereas the pressure at the stagnation point below the particle tends to rotate it clockwise. The torques due to these two forces are seen to be almost equal in magnitude. The particle's approach to the wall is always along a trajectory in which the point of closest separation from the wall is below the particle's centre of mass. As the particle gets close to the wall, the pressure at this point increases significantly due to the interaction with the wall. From figure 20(d), we see that at  $t = 0.6\tau$  (where  $\tau$  is the period of the tumbling motion) there is a strong contribution to the pressure component of the torque due to this interaction. The fluid squeezing through the narrow gap between the particle and the wall acts to diminish the effect of the torque due to pressure-buildup. However, we see that the magnitude of the torque due to pressure is slightly larger than the counter-acting torque due to viscous stresses. This results in a net positive torque on the particle, rotating it in the anomalous sense. This mechanism could provide a possible explanation for the anomalous rotation of elliptic particles. However as mentioned above, this is a very subtle effect and further studies are needed to provide more insight into the phenomenon.

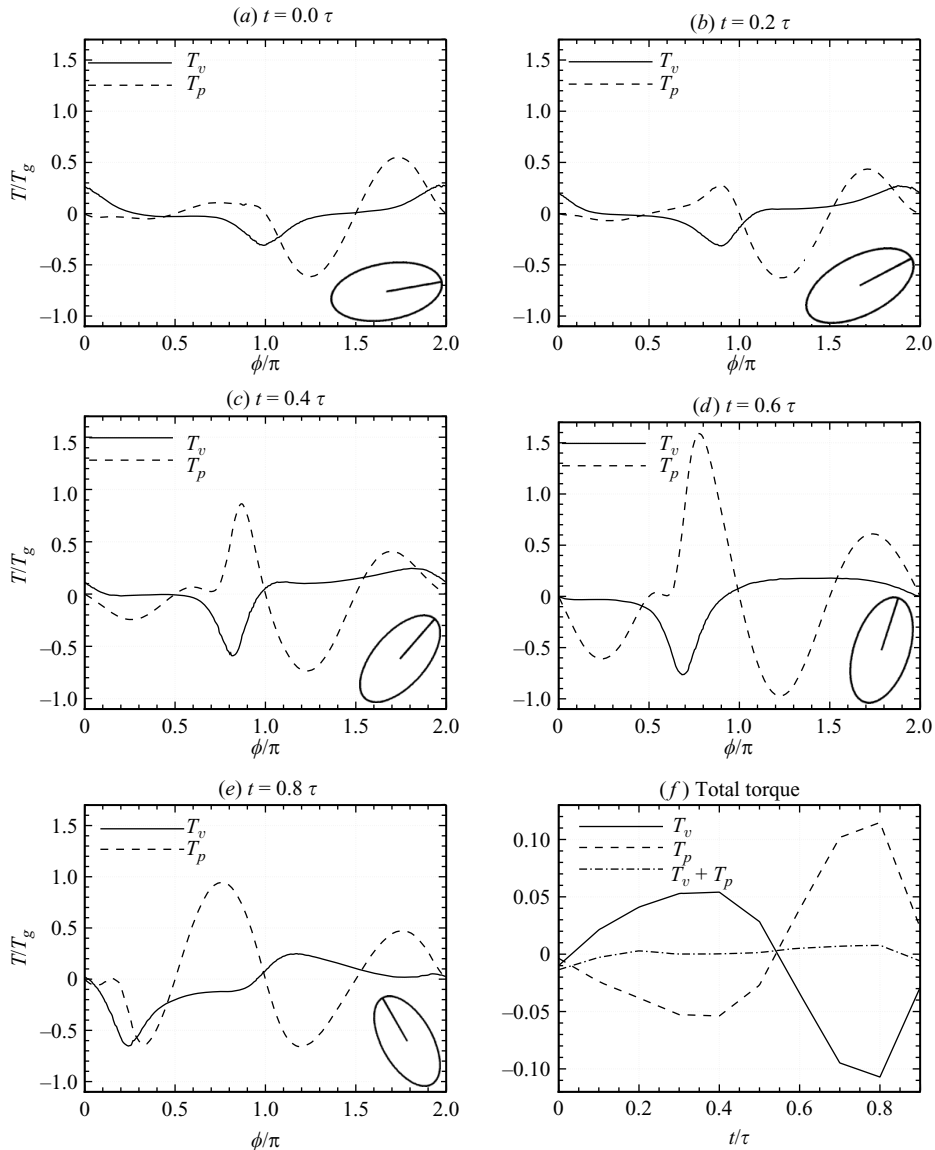


FIGURE 20. (a–e) Distribution of torques (normalized by  $T_g = (\gamma - 1)\rho_f A_p g a$ ) due to pressure and shear forces on the surface of the ellipse as a function of the azimuthal angle  $\phi$  measured counter-clockwise from the major axis shown, at  $t = 0.0, 0.2, 0.4, 0.6$  and  $0.8\tau$  where  $\tau$  is the time period of tumbling motion. (f) The contribution to the total torque from pressure and shear stresses at different times.

## 5. Conclusions

We have presented lattice Boltzmann and finite-element computations of sedimentation of a single two-dimensional elliptical particle in a channel. For all the cases presented in this paper, the results from the LBM are consistent with those obtained using the finite-element method, establishing the LBM as a reliable tool for modelling fluid–solid interactions. For wide channels (where the blockage ratio,  $\beta \geq 2.0$ ) our results are consistent with those reported by other authors. The



simulations show that at low channel blockage ratios, the particle undergoes a series of transitions in the pattern of sedimentation including oscillation, tumbling, horizontal sedimentation, vertical sedimentation and a previously unknown inclined mode of sedimentation where the particle sediments with a non-trivial inclination to the horizontal. We have also shown that for channels with low blockage ratio, the final mode of sedimentation depends sensitively on the initial conditions, specifically the initial angle of orientation whereas for wide channels the sedimentation of the particle was found to be insensitive to the initial conditions.

It was found that the terminal Reynolds number obeys a non-trivial scaling with respect to the aspect ratio of the particle,  $Re \sim \alpha^{-0.7}$ . As of this writing, the reasons behind this scaling are not clear and need further research to understand this behaviour. We also observe the ‘anomalous’ rotation of the elliptical particle where the particle tumbles along the wall with a sense of rotation as if it was rolling up the wall. We have studied the balance of forces and torques acting on the particle during this motion. We find that the anomalous rotation appears to be caused by a subtle effect arising after the cancellation of torques due to pressure and viscous stresses acting on different parts of the ellipse.

The lattice Boltzmann technique used in this paper can be extended without much difficulty to higher Reynolds numbers and simulations involving interactions among multiple particles. One would need to use a hierarchical multi-block scheme to obtain fine resolution in the vicinity of the particle. The experience gained from the research on particle–wall interactions in this paper will help us in more complicated scenarios involving particle–particle interactions.

In the future, we plan to extend this work to three dimensions, where experiments have already confirmed an inclined mode for ellipsoidal particles in tubes (Swaminathan *et al.* 2006) and rotating cylinders (Seddon & Mullin 2007). This is similar to the inclined mode observed by us in the two-dimensional simulations.

The authors would like to thank Professor Renwei Mei for permission to use figure 2 and Professor Andrea Prosperetti, Professor Haiping Fang, Professor A. Ladd and Professor Qingdong Cai for valuable discussions. Zhenhua Xia would like to thank the China Scholarship Council for supporting his visit to Johns Hopkins University. Simulations were done on a cluster computer in the Center for Computational Science and Engineering at Peking University, China and a cluster computer at the Johns Hopkins University supported by NSF Grant Nos. CBET-0320907 and AST-0428325. This work is also supported by Project Nos. 10402001 and 10532010 from the National Natural Science Foundation of China and NSF-DMS-0613085 and NSF-CMMI-0709187 from the National Science Foundation, USA.

#### REFERENCES

- AIDUN, C. K. & DING, E.-J. 2003 Dynamics of particle sedimentation in a vertical channel: period-doubling bifurcation and chaotic state. *Phys. Fluids* **15**, 1612.
- AIDUN, C. & LU, Y. 1995 Lattice boltzmann simulation of solid particles suspended in fluid. *J. Stat. Phys.* **81** (1–2), 49–61.
- AIDUN, C., LU, Y. & DING, E. 1998 Direct analysis of particulate suspensions with inertia using the discrete boltzmann equation. *J. Fluid Mech.* **373**, 287–311.
- ALLEN, M. & TILDESLEY, D. 1987 *Computer Simulation of Liquids*. Clarendon.
- BHATNAGAR, P., GROSS, E. & KROOK, M. 1954 A model for collision processes in gases. I. Small amplitude processes in charged and neutral one-component systems. *Phys. Rev.* **94** (3), 511–525.



- BRADY, J. & BOSSIS, G. 1985 The rheology of concentrated suspensions of spheres in simple shear flow by numerical simulation. *J. Fluid Mech.* **155**, 105–129.
- CHEN, H., CHEN, S. & MATTHAEUS, W. 1992 Recovery of the navier-stokes equations using a lattice-gas boltzmann method. *Phys. Rev. A* **45**, R5339–R5342.
- CHEN, S. & DOOLEN, G. 1998 Lattice boltzmann method for fluid flows. *Annu. Rev. Fluid Mech.* **30**, 329–364.
- CHEN, S., MARTINEZ, D. & MEI, R. 1996 On boundary conditions in lattice boltzmann methods. *Phys. Fluids* **8**, 2527–2536.
- DING, E. & AIDUN, C. 2000 The dynamics and scaling law for particles suspended in shear flow with inertia. *J. Fluid Mech.* **423**, 317–344.
- FANG, H. & CHEN, S. Y. 2004 Lattice boltzmann method for three-dimensional moving particles in a newtonian fluid. *Chin. Phys.* **13** (1), 47–53.
- FANG, H., WANG, Z., LIN, Z. & LIU, M. 2002 Lattice boltzmann method for simulating the viscous flow in large distensible blood vessels. *Phys. Rev. E* **65**, 051925.
- FENG, J., HU, H. & JOSEPH, D. 1994a Direct simulation of initial value problems for the motion of solid bodies in a newtonian fluid Part 1. Sedimentation. *J. Fluid Mech.* **261**, 95–134.
- FENG, J., HU, H. & JOSEPH, D. 1994b Direct simulation of initial value problems for the motion of solid bodies in a newtonian fluid Part 2. Couette and Poiseuille flows. *J. Fluid Mech.* **277**, 271–301.
- FENG, J., HUANG, P. & JOSEPH, D. 1995 Dynamic simulation of the motion of capsules in pipelines. *J. Fluid Mech.* **286**, 201–227.
- FENG, J. & JOSEPH, D. 1995 The unsteady motion of solid bodies in creeping flows. *J. Fluid Mech.* **303**, 83–102.
- FENG, Z. & MICHAELIDES, E. 2004 The immersed boundary-lattice boltzmann method for solving fluid-particles interaction problems. *J. Comput. Phys.* **195**, 602–628.
- FILIPPOVA, O. & HANEL, D. 1997 Lattice-Boltzmann simulation of gas-particle flow in filters. *Comput. Fluids* **26** (7), 697–712.
- FILIPPOVA, O. & HANEL, D. 1998 Grid refinement for lattice bgk models. *J. Comput. Phys.* **147**, 219–228.
- FRISCH, U., D'HUMIERES, D., HASSLACHER, B., LALLEMAND, P., POMEAU, Y. & RIVET, J. 1987 Lattice gas hydrodynamics in two and three dimensions. *Complex Syst.* **1**, 649–707.
- GLOWINSKI, R., PAN, T., HESLA, T., JOSEPH, D. & PERIAUX, J. 2001 A fictitious domain approach to the direct numerical simulation of incompressible viscous flow past moving rigid bodies: application to particulate flow. *J. Comput. Phys.* **169**, 363–426.
- HE, X. & DOOLEN, G. D. 1997 Lattice Boltzmann method on curvilinear coordinates system: flow around a circular cylinder. *J. Comput. Phys.* **134**, 306.
- HE, X. & LUO, L. 1997 Lattice Boltzmann model for the incompressible Navier–Stokes equation. *J. Stat. Phys.* **88** (3–4), 927–944.
- HE, X., LUO, L. & DEMBO, M. 1996 Some progress in lattice Boltzmann method. Part I. Nonuniform mesh grids. *J. Comput. Phys.* **129**, 357–363.
- HÖFLER, K. & SCHWARZER, S. 2000 Navier–Stokes simulation with constraint forces: finite-difference method for particle-laden flows and complex geometries. *Phys. Rev. E* **61**, 7146–7160.
- HU, H. 1995 Motion of a circular cylinder in a viscous liquid between parallel plates. *Theor. Comput. Fluid Dyn.* **7**, 441–455.
- HU, H. 1996 Direct simulation of flows of solid-liquid mixtures. *Intl J. Multiphase Flow* **22** (2), 335–352.
- HU, H., JOSEPH, D. & CROCHET, M. 1992 Direct simulation of fluid particle motions. *Theor. Comput. Fluid Dyn.* **3**, 285–306.
- HU, H. H., PATANKAR, N. A. & ZHU, M. Y. 2001 Direct numerical simulations of fluid–solid systems using the arbitrary Lagrangian–Eulerian technique. *J. Comp. Phys.* **169**, 427–462.
- HUANG, P., FENG, J. & JOSEPH, D. 1994 The turning couples on an elliptic particle settling in a vertical channel. *J. Fluid Mech.* **271**, 1–16.
- HUANG, P., HU, H. & JOSEPH, D. 1998 Direct simulation of the sedimentation of elliptic particles in oldroyd-b fluids. *J. Fluid Mech.* **362**, 297–325.
- INAMURO, T., MAEBA, K. & OGINO, F. 2000 Flow between parallel walls containing the lines of neutrally buoyant circular cylinders. *Intl J. Multiphase Flow* **26**, 1981–2004.

- LADD, A. 1994a Numerical simulations of particulate suspensions via a discretized Boltzmann equation. Part 1. Theoretical foundation. *J. Fluid Mech.* **271**, 285–309.
- LADD, A. 1994b Numerical simulations of particulate suspensions via a discretized Boltzmann equation. Part 2. Numerical results. *J. Fluid Mech.* **271**, 311–339.
- LADD, A. & VERBERG, R. 2001 Lattice-Boltzmann simulations of particle-fluid suspensions. *J. Stat. Phys.* **104** (5–6), 1191–1251.
- LAI, M.-C. & PESKIN, C. S. 2000 An immersed boundary method with formal second-order accuracy and reduced numerical viscosity. *J. Comput. Phys.* **160**, 705–719.
- LI, H., FANG, H., LIN, Z., XU, S. & CHEN, S. 2004a Lattice Boltzmann simulation on particle suspensions in a two-dimensional symmetric stenotic artery. *Phys. Rev. E* **69** (3), 031919.
- LI, H., LU, X., FANG, H. & QIAN, Y. 2004b Force evaluations in lattice Boltzmann simulations with moving boundaries in two dimensions. *Phys. Rev. E* **70**, 026701.
- LIU, Y. J., NELSON, J., FENG, J. & JOSEPH, D. D. 1993 Anomalous rolling of spheres down an inclined plane. *J. Non-Newtonian Fluid Mech.* **50**, 305.
- M McNAMARA, G. & ZANETTI, G. 1988 Use of the boltzmann equation to simulate lattice-gas automata. *Phys. Rev. Lett.* **61** (20), 2332–2335.
- MEI, R., LUO, L. & SHYY, W. 1999 An accurate curved boundary treatment in the lattice Boltzmann method. *J. Comput. Phys.* **155**, 307–330.
- MEI, R., YU, D., SHYY, W. & LUO, L. 2002 Force evaluation in the lattice Boltzmann method involving curved geometry. *Phys. Rev. E* **65**, 041203.
- MITTAL, R. & IACCARINO, G. 2005 Immersed boundary methods. *Annu. Rev. Fluid Mech.* **37**, 239–261.
- NGUYEN, N. Q. & LADD, A. J. C. 2002 Lubrication corrections for lattice-Boltzmann simulations of particle suspensions. *Phys. Rev. E* **66**, 046708.
- PROSPERETTI, A. & OGUZ, H. 2001 Physalis: a new  $o(n)$  method for the numerical simulation of disperse systems: potential flow of spheres. *J. Comput. Phys.* **167**, 196–216.
- QI, D. 1999 Lattice-Boltzmann simulations of particles in non-zero-Reynolds-number flows. *J. Fluid Mech.* **385**, 41–62.
- QI, D., LUO, L., ARAVAMUTHAN, R. & STRIEDER, W. 2002 Lateral migration and orientation of elliptical particles in poiseuille flows. *J. Stat. Phys.* **107** (1–2), 101–120.
- QIAN, Y., D'HUMIERES, D. & LALLEMAND, P. 1992 Lattice bgk models for Navier–Stokes equation. *Europhys. Lett.* **17** (6), 479–484.
- RUSSEL, W. B., HINCH, E. J., LEAL, L. G. & TIEFFENBRUCK, G. 1977 Rods falling near a vertical wall. *J. Fluid Mech.* **83**, 273–287.
- SEDDON, J. R. T. & MULLIN, T. 2007 The motion of a prolate ellipsoid in a rotating Stokes flow. *J. Fluid Mech.* **583**, 123–132.
- SUGIHARA-SEKI, M. 1993 The motion of an elliptical cylinder in channel flow at low Reynolds numbers. *J. Fluid Mech.* **257**, 575–596.
- SWAMINATHAN, T. N., MUKUNDAKRISHNAN, K. & HU, H. H. 2006 Sedimentation of an ellipsoid inside an infinitely long tube at low and intermediate Reynolds numbers. *J. Fluid Mech.* **551**, 357–385.
- UHLMANN, M. 2005 An immersed boundary method with direct forcing for the simulation of particulate flows. *J. Comput. Phys.* **209**, 448–476.
- YU, D., MEI, R., LUO, L.-S. & SHYY, W. 2003 Viscous flow computations with the method of lattice Boltzmann equation. *Prog. Aero. Sci.* **39**, 329–367.
- YU, D., MEI, R. & SHYY, W. 2002 A multi-block lattice Boltzmann method for viscous fluid flows. *Intl J. Numer. Meth. Fluids* **39**, 99–120.